High Performance Medical Robot Requirements and Accuracy Analysis

C. Mavroidis[1], J. Flanz[2], S. Dubowsky [3], P. Drouet[4] and Michael Goitein[2]

[1] Department of Mechanical and Aerospace Engineering, Rutgers University
98 Brett Road, Room B-217, Piscataway, NJ 08854, USA
Tel 732-445-0732, Fax 732-445-3124, email mavro@jove.rutgers.edu

[2] Northeast Proton Therapy Center, Massachusetts General Hospital
Boston, MA 02114 USA, Tel 617-724-9528, Fax 617-724-9532

[3] Massachusetts Institute of Technology, Department of Mechanical Engineering
Cambridge, MA 02139, USA, Tel 617-253-2144, Fax 617-258-7881

[4] Laboratoire de Mécanique des Solides, Université de Poitiers
Bât. SP2MI, 86960 Futuroscope, FRANCE, Tel 05.49.49.65.00

Abstract

The treatment of disease using particle beams requires highly accurate patient positioning. Patients must be well immobilized and precisely aligned with the treatment beam to take full advantage of the dose localization potential. Robots can be used as high accuracy patient positioning systems. In this paper, the first such implementation using robotics techniques for patient positioning will be discussed. This robot is being developed for the Northeast Proton Therapy Center at the Massachusetts General Hospital. The unique requirements and design characteristics of the patient positioning system are presented. Of special interest is the system's patient positioning accuracy. A systematic methodology to perform the error analysis of serial link manipulators and its application to the PPS is described. Experimental measurements that verified the validity of the method are shown.

1 INTRODUCTION

The application of robotic technology in clinical medicine has recently been a very active research area [7]. Robotic systems have been proposed to perform surgical procedures such as knee arthoplasty, neurosurgery or eye surgery [16, 24]. In most of these surgical operations the robot will serve as an aid to the doctor or as an extension of the doctor capabilities. Other possible applications of robotic systems in clinical medicine, include miniature robots for endoscopic diagnostic and surgical interventions [22] and robots as rehabilitation or aid systems to people with disabilities [14, 18]. Most of these medical robotic systems are still research devices and very few of

them have been used in a real medical application where they are in contact with a patient. A major reason for this is that current medical robots can not solve in a repeatable and reliable way two important problems: ultra-high positioning robot accuracy and patient safety.

In this paper, a new important medical application of robotic systems is studied: a high accuracy robotic patient positioning system in radiation therapy. The Northeast Proton Therapy Center (NPTC) is now being constructed at the Massachusetts General Hospital (MGH) [11, 23]. This cancer research and treatment facility has a new advanced proton therapy system. The NPTC is scheduled to begin operations with patients in 1998.

A major component of the system is its robotic patient positioning system (PPS). This system will be used to position a patient in a high energy proton beam delivered from a rotating gantry structure. The support and alignment of the patient is a crucial element in the overall system. Patients must be well immobilized and precisely aligned with the treatment beam to take full advantage of the dose potential of this facility. A patient positioning system (PPS), when used with a gantry beam, must permit proton beam entry from any oblique direction, without danger of collision with the gantry or beam shaping hardware. For the NPTC, the required absolute positioning accuracy of the PPS is ±0.5 mm. Larger errors may be dangerous to the patient [25]. So, the accuracy of the PPS is critical. Further, the ability to predict the accuracy as a function of the system configuration during the system design was important and this is the subject of this research.

Considerable research has been performed in the area of kinematic error analysis of robotic manipulators and machine tools [15, 17, 21, 32]. Error models have been developed based on screw theory, homogeneous matrices, Denavit and Hartenberg coordinates, and Jacobian matrices [3, 19, 20, 30, 35]. Some studies have considered the effects of manipulator joint errors [1, 29], while others were focused on the effects of link dimensional errors [9, 31]. Some generalized methods have been proposed which include non-geometric errors such as thermal effects [8, 27]. Error models have been developed specifically for use in the calibration of manipulators [2, 33]. Researchers have studied methods to predict the error sensitivity of manipulator design [4, 28] and

others have done work to find the optimal configurations to reduce the manipulator errors by calibration [34]. All these methods, from the theoretical point of view, can solve most of the problems related to the manipulator error analysis. However, when the goal is to build a generic software tool to perform the error analysis of any six degree of freedom manipulator in a systematic and unified way, adjustments to these methods need to be made.

This paper has two objectives. First, to present the clinical requirements of the NPTC robotic patient positioning system. This robot manipulator can serve as a general case study of mechatronic design of medical manipulators. The second goal of the paper, is to show how based on existing theories, a generic software tool is built to perform the error analysis of any six degree of freedom manipulator in a systematic way, incorporating any type of physical error sources that may exist, such as geometric errors, backlash, joint or link deflections. This tool is applied to the performance evaluation of the NPTC medical robot and simulation results are presented. Experimental verification of the computer predictions are shown.

2 DESIGN REQUIREMENTS

The general schematic of the system at the treatment room is shown in Figure 1. At the treatment room the beam delivery system is attached to a large rotating gantry. The patient is placed on a couch attached at the end effector of the robotic patient positioning system.

The gantry rotation is required to achieve various angles of beam penetration into the patient body. The point of intersection of the gantry axis of rotation and of the beam is called “isocenter” and it is a very important point of the system since, in classical robot terminology, it is the desired “robot end-effector location.” The PPS should bring the patient into the gantry enclave and place the patient body in such a position so that the tumor and the isocenter are coincident. Due to the size of the gantry, it is necessary that the PPS be of a cantilevered design to bring the patient's target to the isocenter. In Figure 2, the side view of the treatment room with the gantry, nozzle and patient positioning system is shown. Information on other components of the system can be found in [10,11].

There are five basic clinically motivated requirements that have been considered: a) clinical accuracy requirements, b) minimum patient movement, c) minimum treatment time, d) maximum patient workspace and e) safety. These requirements lead to the following design specifications for the PPS:

1. The patient support system must be able to support at least 98% of all potential patients in such a way that all points in any conceivable target can be accurately and in a repeatable way aligned to the beam to within ±0.5mm of their intended position.
2. The couch and gantry should have 6 relative degrees of freedom: 3 translations and 3 rotations.
3. The PPS can present any point of a 50cm x 50cm x 40cm (vertical) working volume on the couch at the gantry isocenter.
4. The PPS should present any point in a supine patient at gantry isocenter with the patient's orientation in the horizontal plane at any angle within a ±95° range.
5. The couch structure must be larger than the patient and provide the space for the constraints that hold the patient in accurate position with respect to the couch.
6. Space must be allowed for ancillary equipment, such as necessary life support equipment, that must be attached to the couch.
7. A buffer zone space between components must be allowed to accommodate the overtravel that occurs between the time that an interlock violation is detected and the PPS actually decelerates to a stop.

3 THE PATIENT POSITIONING SYSTEM

The design requirements described in Section 2 lead to the system shown in Figure 3. It is a six degree of freedom manipulator being developed by General Atomics [13]. The first three joints are prismatic. The maximum travel for these joints is 225.6 cm for the lateral (X) axis, 56 cm for the vertical (Y) axis, and 147.3 cm for the longitudinal (Z) axis. The last three joints are revolute joints. The first revolute joint has an axis of rotation parallel to the Y axis and can rotate ±90°. The last two joints are used for small corrections around an axis of rotation parallel to the Z (i.e. roll) and X (i.e. pitch) axes, respectively, and have a maximum rotation angle of ±3°. All of the joints are actuated by stepper motors. The connecting members and supporting structures of the

PPS are made out of steel. The manipulator's "end-effector" is a couch which supports the patient in a supine position. The design accommodates supine patients up to 188 cm in height and 300lbs in weight in normal operations.

The overall PPS operating envelope is a major driver of the gantry design in that it sizes the minimum inner diameter of the front gantry bearing ring. Since the patient must be rotated 90° with respect to the gantry axis of rotation, the radius of the gantry ring must be substantially larger than the height of the patient. The patient couch assembly mounts directly to a load cell. The load cell provides a means of measuring a patient's weight and the center of gravity position of the couch during treatment. The load cell will acquire the data necessary for an algorithm to compensate for the deflection caused by the variable weight and location of the patient on the PPS.

4 SYSTEMATIC ERROR ANALYSIS OF MANIPULATORS

The PPS should be an ultra-high accuracy robot manipulator. Even small mechanical or measurement errors can create substantial end-effector positioning errors compared to the very small accuracy specifications of the system. A systematic error analysis method has been developed to analyze the PPS design. The method is general and can be applied to any serial link manipulator. While it is based on classical concepts used in error analysis of mechanical systems, the method presented here, is formulated in a very simple and straight forward manner which makes it a practical solution for commercial applications and software development.

There are many possible sources of errors in a manipulator. These errors are referred to as "physical errors", to distinguish them from "generalized errors" which are defined later. The main sources of physical errors in a manipulator are:

· **Machining errors:** These errors are resulting from machining tolerances of the individual mechanical components that are assembled to build the robot.

· **Assembly:** These errors include linear and angular errors that are produced during the assembly of the various manipulator mechanical components.

· **Deflections:** Link and joint flexibility can cause elastic deformations of the structural members of the manipulator, resulting in large end-effector errors, especially in long reach manipulator systems. Local material deformations can also be another source of end-effector errors.

· **Measurement and Control:** Measurement, actuator, and control errors that occur in the control systems will create end-effector positioning errors. The resolution of encoders and stepper motors are examples of this type of error.

· **Joint errors:** These errors include bearing run-out errors in rotating joints and rail curvature errors in linear joints.

· **Clearances:** Backlash errors can occur in the motor gear box and in the manipulator joints.

In most cases, the physical errors are usually very small. However, they can be amplified by the system to cause large errors at the end-effector. As a result, it is essential to identify those errors in the system which significantly influence the end-effector positioning accuracy.

Errors can be distinguished into “repeatable” and “random” errors [26]. Repeatable errors are errors whose numerical value and sign are constant for each manipulator configuration. An example of a repeatable error is an assembly error. Random errors are errors whose numerical value or sign changes unpredictably. At each manipulator configuration, the exact magnitude and direction of random errors cannot be uniquely determined, but only specified over a range of values. An example of a random error is the error that occurs due to backlash of an actuator gear train.

4.1 Kinematic Model Without Errors

Classical kinematic analysis of a manipulators requires the definition of reference frames at the manipulator base, end-effector, and at each of the joints [5]. For a six degree of freedom manipulator, 7 reference frames F_i (i ranging from 0 to 6) are defined. Generally, these frames are characterized using the Denavit and Hartenberg method [5]. The position and orientation of a reference frame F_i with respect to the previous reference frame F_{i-1} is defined with a 4x4 matrix $\mathbf{A}_i$ that has the general form:

$$\mathbf{A}_i = \begin{pmatrix} \mathbf{R}_i & \mathbf{T}_i \\ 0 & 1 \end{pmatrix} \tag{1}$$

The $\mathbf{R}_i$ term is a 3x3 orientation matrix composed of the direction cosines of frame F_i with respect to frame F_{i-1} and $\mathbf{T}$ is a 3x1 vector of the coordinates of center O_i of frame F_i in F_{i-1}. (Bold lettered variables represent vectors or matrices.) The elements of matrices $\mathbf{A}_i$ depend on the geometric parameters of the manipulator and the manipulator configuration parameters $\mathbf{q}$. For a 6R manipulator, $\mathbf{q}$ is composed of the six manipulator joint angles.

The position and orientation of the end-effector frame F_6, with respect to the inertial reference frame F_0, is represented by the homogeneous matrix $\mathbf{A}_T$. The elements of $\mathbf{A}_T$ depend on the 3 position parameters (i.e. the three coordinates of the origin of F_6 in F_0) and 3 orientation parameters which are the euler angles of frame F_6 with respect to frame F_0. These six parameters are also represented with a 6x1 vector $\mathbf{X}_T$.

At this point the superscript i will be added to $\mathbf{X}_T$ to denote the ideal position of F_6 with respect to frame F_0, if no errors exist in the manipulator. The superscript r, will be used later to denote the real or actual position of F_6 when errors exist. The matrix $\mathbf{A}_T$ is formed by multiplying all of the $\mathbf{A}_i$ matrices [5]:

$$\mathbf{A}_T = \mathbf{A}_1\mathbf{A}_2 \ldots\ldots \mathbf{A}_6 \tag{2}$$

From Equation (2), known as the "loop closure equation," six scalar equations are obtained to calculate the end-effector coordinates $\mathbf{X}_T^i$ when the configuration parameters $\mathbf{q}$ are known:

$$\mathbf{X}_T^i = \mathbf{f}^i(\mathbf{q}, \mathbf{s}) \tag{3}$$

The vector $\mathbf{f}^i$ is a non-linear function of the configuration parameters, $\mathbf{q}$, and a vector of the manipulator structural parameters $\mathbf{s}$. Equation (3) represents the relationship between the manipulator's configuration parameters and the position and orientation coordinates of its end-effector. This is known as the "manipulator direct kinematic model." This model is often used in a manipulator controller to calculate the end-effector inertial coordinates from system joint displacements. A

"manipulator inverse kinematic model" is used to calculate the configuration parameters to achieve a desired end-effector location and orientation.

If the manipulator has errors, Equation (3) will not accurately represent the system's direct kinematics. Using equation (3) to position the manipulator end-effector, the manipulator would placed it in a different position then the desired one. In the following section, equations are formulated to accurately represent the relationship between configuration parameters **q** and end-effector coordinates $\mathbf{X}_T$ when errors exist in the manipulator.

4.2 Generalized Errors

Physical errors change the geometric properties of a manipulator. As a result, the frames defined at the manipulator joints are slightly displaced from their expected, ideal locations. In Figure 4, frame F_i is shown in the ideal location F_T^i and in its real location F_T^r due to errors.

The position and orientation of a frame F_T^r with respect to its ideal location F_T^i is represented by a 4x4 homogeneous matrix $\mathbf{E}_i$. The rotation part of matrix $\mathbf{E}_i$ is the result of the product of three consecutive rotations e_{si}, e_{ri}, e_{pi} around the Y, Z and X axes respectively. (These are the Euler angles of F_T^r with respect to F_T^i.) The subscripts s, r, and p represent spin (yaw), roll, and pitch, respectively. The translational part of matrix $\mathbf{E}_i$ is composed of the 3 coordinates e_{xi}, e_{yi} and e_{zi} of point O_T^r in F_T^i.

The 6 parameters e_{xi}, e_{yi}, e_{zi}, e_{si}, e_{ri} and e_{pi} are called here "generalized error" parameters. For a six degree of freedom manipulator, there are 36 generalized errors which can be written in vector form as $\varepsilon=[\ldots,.e_{xi}, e_{yi}, e_{zi}, e_{si}, e_{ri}, e_{pi},..]$, with i ranging from 1 to 6. Since the physical errors are small, the generalized errors e_{xi}, e_{yi}, e_{zi}, e_{si}, e_{ri} and e_{pi} are also small, so a first order approximation can be applied to their trigonometric functions and products. Matrix $\mathbf{E}_i$, after the first order approximation, has the form:

$$\mathbf{E}_i = \begin{pmatrix} 1 & -e_{ri} & e_{si} & e_{xi} \\ e_{ri} & 1 & -e_{pi} & e_{yi} \\ -e_{si} & e_{pi} & 1 & e_{zi} \\ 0 & 0 & 0 & 1 \end{pmatrix} \tag{4}$$

The generalized errors can easily be calculated from the physical errors. Consider the simple example shown in Figure 5.

Two frames, F_1 and F_2, are connected by two structural members *A* and *B* that should be aligned. During the assembly of *A* and *B*, a linear error d or an angular error ψ is introduced. The linear error will cause a translation of frame F_2, and the angular error will cause both an angular displacement and a linear displacement of F_2. In Figure 5, the generalized errors are calculated for this example. The generalized errors for an entire manipulator can also be calculated from the physical errors by a similar process.

4.3 Kinematic Model With Errors

The end-effector position and orientation error $\Delta\mathbf{X}$ is defined as the 6x1 vector that represents the difference between the real position and orientation of the end-effector and the ideal or desired one:

$$\Delta\mathbf{X} = \mathbf{X}_T^r - \mathbf{X}_T^i \tag{5}$$

Here, $\mathbf{X}_T^r$ and $\mathbf{X}_T^i$ are the 6x1 vectors that represent the position and orientation of the end-effector reference frame (F_6) in the inertial reference system (F_0) for the real and ideal case, respectively. The vector $\Delta\mathbf{X}$ must be calculated for a given set of physical errors. Many physical errors may not play an important role in end-effector error. The first step in this analysis is to determine which physical errors significantly influence the end-effector positioning accuracy. A manipulator error model, which maps the manipulator's physical errors into generalized error components, and then into end-effector errors is used. If the end-effector error is greater than the desired tolerance, the identified physical errors can either be corrected or the manipulator controller can be pro-

grammed to compensate for the errors if the errors are repeatable. A complete discussion of these compensation algorithms is beyond the scope of this paper. In this section, a general method to obtain the error model is described.

When the generalized errors are considered in the model, the manipulator loop closure equation takes the form:

$$\mathbf{A}_T = \mathbf{A}_1\mathbf{E}_1\mathbf{A}_2\mathbf{E}_2\ldots\ldots\mathbf{A}_6\mathbf{E}_6 \tag{6}$$

As in Section 4.1, the end-effector position and orientation coordinates, $\mathbf{X}_T^r$ can be calculated from Equation (6):

$$\mathbf{X}_T^r = \mathbf{f}^r(\mathbf{q}, \varepsilon, \mathbf{s}) \tag{7}$$

Here, $\mathbf{f}$ is a vector non-linear function of the configuration parameters $\mathbf{q}$, the vector of the generalized errors ε, and the vector of the structural parameters $\mathbf{s}$. Equation (7) is called the "direct kinematic error model".

In the error analysis of a manipulator, the end-effector position and orientation errors need to be calculated as a function of the generalized errors. This is required in order to understand the effect of the physical errors on the end-effector positioning accuracy of the manipulator. Since the generalized errors are small, $\Delta\mathbf{X}$ can be calculated by the following linear equation in ε:

$$\Delta\mathbf{X} = \mathbf{J}_e\,\varepsilon \tag{8}$$

Here, $\mathbf{J}_e$ is the 6x36 Jacobian matrix of the function $\mathbf{f}^r$ defined in Equation (7) with respect to the elements of the generalized error vector ε. Equation (8) is called the "manipulator error model". The elements of $\mathbf{J}_e$ are defined as:

$$\mathbf{J}_e[i,j] = \frac{\partial \mathbf{f}[i]}{\partial \varepsilon[j]} \tag{9}$$

where i ranges from 1 to 6 and j ranges from 1 to 36. Matrix $\mathbf{J}_e$ is called the "manipulator error matrix."

4.4 Symbolic Calculation

A computer program has been developed to calculate the manipulator error model and perform the error analysis of any serial link manipulator. The outline of the software is shown in Figure 6. The manipulator error matrix is calculated analytically using the symbolic calculation software package *Maple* . The inputs to the program are homogeneous matrices $\mathbf{A}_i$ that represent the manipulator's nominal geometric properties. The output of the *Maple* program is a C script containing the analytical algebraic forms of the error matrix $\mathbf{J}_e$. Then, a *Matlab* program reads the input files that define the numerical values of the configuration parameters $\mathbf{q}$, the generalized errors ε, and the structural parameters $\mathbf{s}$ and executes the C-script file that contains the numerical value of $\mathbf{J}_e$. From Equation (8), the treatment point error vector $\Delta\mathbf{X}$ is then calculated.

5 PERFORMANCE EVALUATION OF THE PPS

A large set of potential physical error sources has been identified for the PPS design. The computer program presented in Section 4.4 has been used. Nominal geometric parameters such as link lengths, twist angles and offsets were obtained from autocad drawings of the PPS. Values of the physical errors of the PPS were determined using information provided by the manufacturers of each component of the PPS and by General Atomics.

5.1 Single Error Analysis

Each physical error is studied separately, in order to determine which physical errors induce large treatment errors. It was found that the angular treatment point errors resulting from the physical errors considered were very small from a medical point of view and could therefore be ignored. However, the linear displacement error induced by some physical errors was found to be very significant. The amplification of small physical errors into large treatment point errors is primarily caused by the long cantilever utilized in the design of this system. In this section, examples of these errors are presented.

- **Base Rail Curvature**

The first three joints of the PPS are prismatic joints, for which the moving elements slide on rails. The base rail is considered in this example (see Figure 3.) One of the possible physical errors associated with the base rail is the curvature of the rail. This is a repeatable error. A representation of the rail error is shown in Figure 7. The error is assumed to be a sinusoidal function of the travel d_1 of the prismatic joint. The rail has a maximum angular deviation of 0.000125 radians and a maximum linear error of 0.2 mm over its total length.

The generalized errors associated with these physical error are found to be:

$$e_{z1} = -0.000062\, d_1 - 0.060706 \sin\left(\frac{\pi}{1600\, d_1}\right)$$

$$e_{s1} = -0.000062\, d_1 - 0.000119 \cos\left(\frac{\pi}{1600\, d_1}\right)$$

In Figure 8, the treatment point error for the rail error source is shown for Z and X directions. For this particular physical error, there is no error in the Y direction. These treatment point errors are calculated over the span of the manipulator workspace, which is defined as the range of motions which will keep the proton beam within the treatment volume. The treatment volume is a 50x50x40 cm volume on the couch within which the treatment point must be located. The maximum treatment point error due to base rail curvature is 0.22 mm in the X direction and 0.08 mm in the Z direction. This error is considered to be significant because, in some configurations, almost 50% of the total accuracy specification is reached by just this error alone. However it is a repeatable error, so that the system software can compensate for it if it can be well characterized.

- **Encoder Resolution**

Encoders are used on each axis of motion. It has been estimated that the encoder used on the revolute axis (see Figure 3,) has a resolution of ±0.000063 radians. This is a random error, since the value and the sign of the encoder measurement error cannot be exactly determined. Hence it is important that its effect be well understood and quantified, as it is not possible to compensate its effect with a simple calibration procedure.

The treatment point error in X and Z directions due to this physical error on the spin axis is shown in Figure 9. The maximum error in each direction is 0.074 mm, which is considered to be a significant error because as it can not be corrected by a compensation algorithm, it will be present and it will affect the repeatability (relative accuracy) of the system.

- **Deflections - Elastic Deformations**

Deflections and elastic deformations of various structural members of the PPS are another significant source of errors. Deflections of the arm, vertical post, and couch (see Figure 3,) along with elastic deformations of the bearings, rails, and lead screws can occur. In this example, the deflection of the arm is studied. This is a repeatable error. The arm was modeled as an elastic beam. From classical beam theory [6], the corresponding generalized errors have been calculated as functions of the configuration parameters. Using the error model of the PPS, the treatment error is calculated over the manipulator workspace. The results of this calculation are shown in a three dimensional diagram in Figure 10.

The maximum error is 0.12 mm in the X direction, 0.44 mm in the Y direction, and 0.25 mm in the Z direction.

These results show that the deflection of the PPS structural members are major sources of inaccuracy. Based on these results, the addition of a load cell to the PPS design has been decided. The load cell will be mounted at the end of the PPS arm. The measurements from the load cell will be used in a deflection compensation algorithm.

5.2 Combined Error Analysis

Figure 11 shows the treatment point error calculation where the identified physical errors are assumed to be present. Repeatable errors have been summed arithmetically, assuming that the sign of the errors is known. A root mean square sum (RMS) has been used for random errors. It was found that an uncalibrated PPS will have a maximum positioning error of 5.48 mm, as defined by the radius of the sphere that includes all of the treatment point errors shown in Figure 11. This error is significantly greater than the maximum allowable tolerance of ±0.5 mm. However, many

repeatable errors can be corrected by using a compensation algorithm. It is assumed that a correction algorithm can be developed which will largely correct for repeatable errors. Based on some calculations, it has been estimated that due to uncomplete compensation of repeatable errors the residual accuracy of the PPS becomes ±0.25 mm. Random errors cannot be corrected. The RMS sum of all random was calculated to be ±0.1 mm. Total prediction of the system absolute accuracy when a calibration algorithm is used is ±0.35 mm.

6 EXPERIMENTAL VERIFICATION

The accuracy and repeatability of the PPS were measured experimentally using a Leica 3D Laser Tracking System. Three targets were placed on the couch at the positions P_1, P_2 and P_3, shown in Figure 12. The targets are located about 10mm above the couch. The position accuracy of the measurements is approximately 0.04mm.

A reference frame F_T is fixed to the couch (see Figure 12). The intersection point of the plane (P_1 P_2 P_3) with the Y axis of the fixed reference frame is called O_T. A fixed reference frame, F_o, is used to express the coordinates of all points. When the PPS is at its home configuration (all joint variables set equal to zero) the reference frames F_T and F_o are coincident.

The location of a tumor on a patient, defined as the Nominal Treatment Point (NTP), is specified in the frame coordinate F_T. For the results presented below, the NTP coordinates in F_T are taken as (0, 840, -90) mm.

For more than 700 cases (at different configurations of the PPS and using different weights) the location of points P_1, P_2 and P_3 in frame F_o is measured and the NTP coordinates in frame F_o calculated. From the system kinematic model with no errors (see Section 4.1), the ideal coordinates of NTP were calculated and subtracted from the experimentally measured values to yield the vector $\Delta\mathbf{X}$.

In this work, 450 measurements were used to evaluate the basic accuracy of the PPS. Two different payloads were considered: one with no weight and another with a 154 lbs weight at the center of the treatment area. The PPS configurations used were grouped into two sets:

Set a) *Treatment Volume*. The 8 vertices of the treatment volume (see Figure 3) are reached with the NTP with the angle of the rotary joint taking values from -90° to 90° with a step of 30°, for a total of 112 configurations.

Set b) *Independent Motion of Each Axis*. Each axis is moved independently while all other axes are held at the home (zero) values. The step of motion for the first axis is 50 mm, for the second 20 mm, for the third 25mm and for the rotary joint 5°, resulting in 338 configurations.

The PPS positioning accuracy combining the two sets is shown in Figure 13. It is clearly seen that in spite of the high quality of the PPS physical system, its accuracy is of the order of ±5mm. These measurements verified very accurately the computer error predictions.

The repeatability error of the PPS was also calculated. A total of 270 measurements were taken with zero payload weight. Figure 14 shows the distributions of the repeatability error for each axis. The repeatability error can be seen to be less than 0.15mm (3σ) which is very close to the ±0.1 mm repeatability prediction obtained by the computer simulation program.

7 CONCLUSIONS

In this paper, the design and error analysis of a new ultra-high accuracy medical robot has been presented. This robot manipulator is part of a proton therapy system for the treatment of cancer that is now being installed at the Northeast Proton Therapy Center of the Massachusetts General Hospital. Currently, the Patient Positioning System is assembled and initial performance tests are being held. It is expected that the NPTC will start treating patients at the end of 1998.

8 ACKNOWLEDGMENTS

The information provided by General Atomics, San Diego, CA and Ion Beam Applications, Louvain-La-Neuve, Belgium is acknowledged and appreciated.

9 REFERENCES

1. Benhabib, B., Fenton, R. and Goldenberg, A.: "Computer-Aided Joint Error Analysis of Robots." *IEEE Journal of Robotics and Automation* **RA-3**(4): 317-322, 1987.
2. Broderick, P. and Cirpa, R.: "A Method for Determining and Correcting Robot Position and Orientation Errors Due to Manufacturing." *Transactions of the ASME, Journal of Mechanisms, Transmissions and Automation in Design,* **110**: 3-10, 1988.
3. Chen, J. and Chao L.: "Positioning Analysis for Robot Manipulators With All Rotary Joints." *Proceedings of the 1986 IEEE Robotics and Automation Conference*, **2**: 1011-1016, 1986.
4. Cleghorn, W., Fenton, R. and Fu, J.: "Optimum Tolerancing of Planar Mechanisms Based on an Error Sensitivity Analysis." *Transactions of the ASME, Journal of Mechanical Design,* **115**: 306-313, 1993.
5. Craig, J.: *Introduction to Robotics: Mechanics and Control*, Addison Willey, 1989.
6. Crandall, S., Dahl, N. and Lardner, T.: *An Introduction to the Mechanics of Solids*, McGraw-Hill Book Company, 1978.
7. Dario P., Guglielmelli E., Allotta B. and Carrozza M.: “Robotics for Medical Applications,” *IEEE Robotics and Automation Magazine*, 44-55, September, 1996.
8. Donmez, M., Liu, C. and Baras, M.: "A Generalized Mathematical Model for Machine Tool Errors." *ASME Publications: Modeling, Sensor and Control in Manufacturing Processes* : 231-243, 1988.
9. Ferreira, P. and Liu, R.: "An Analytic Quadratic Model for the Geometric Error of A Machine Tool." *Journal of Manufacturing Systems*, **5**(1): 51-62.
10. Flanz, J., : “Large Medical Gantries.” *Proceedings of the 1995 Particle Accelerator Conference*, April, 1995.
11. Flanz, J. et al.: "Overview of the MGH-Northeast Proton Therapy Center: Plans and Progress." *Nuclear Instruments and Methods in Physics Research B,* **99**: 830-834, 1995.

12. Flanz, J., et al.: “Design Approach for a Highly Accurate Patient Positioning System for NPTC.” *Proceedings of the PTOOG XXV and Hadrontherapy Symposium*, Belgium, September, 1996.

13. General Atomics: *Patient Positioner Preliminary Design Documents*, 1995.

14. Hashino S., “Aiding Robots,” *Advanced Robotics*, **7**:1:97-103, 1991.

15. Hollerbach, J.: "A Survey of Kinematic Calibration." *Robotics Review*, Khatib O. et al editors, Cambridge, MA; MIT Press, 1988.

16. Hunter W., et al.: “Ophthalmic Microsurgical Robot and Surgical Simulator,” Proceedings of the 1995 SPIE Conference, Boston, MA, pp. 184-190, 1995.

17. Kirdena, V. and Ferreira, P.: "Mapping the Effects of Positioning Errors on the Volumetric Accuracy of Five-Axis CNC Machine Tools." *International Journal of Machine Tools in Manufacturing*, **33**(3): 417-437, 1993.

18. Leifer L.: “Rehabilitative Robots,” *Robotic Age*, May/June, 1981.

19. Lin, P. and Ehmann, K.: "Direct Volumetric Error Evaluation for Multi-Axis Machines:" *International Journal for Machine Tools in Manufacturing*, **33** (5): 675-693, 1993.

20. Mirman, C. and Gupta, K.: "Identification of Position Independent Robot Parameter Errors Using Special Jacobian Matrices." *International Journal of Robotics Research*, **12**(3): 288-298, 1993.

21. Mooring, B., Roth, Z., and Driels, M.: *Fundamentals of Manipulator Calibration*. New York; John Willey & Sons, 1991.

22. Narumiya H.: “Micromachine Technology: Intraluminal Diagnostic and Therapeutic System,” *Proceedings of the 1993 Workshop on Micromachine Technologies and Systems*, pp. 60-65, Tokyo, Japan, October, 1993.

23. NPTC, Web Page of the Northeast Proton Therapy Center at the Massachusetts General Hospital, http://www.mgh.harvard.edu/depts/nptc.htm, 1996.

24. Paul H. et al.: “Development of a Surgical Robot for Cementless Total Hip Arthoplasty,” *Clinical Orthopaedics*, **285**:57-66, 1992.

25. Rabinowitz, I. et al: "Accuracy of Radiation Field Alignment in Clinical Practice." *International Journal of Radiation Oncology, Biology and Physics*, **11**: 1857-1867, 1985.

26. Slocum, A.: *Precision Machine Design*.. Englewood Cliffs, 1992.

27. Soons, J., Theus, F. and Schellekens, P.: "Modelling the Errors of Multi-axis Machines: A General Methodology." *Precision Engineering,* **14**(1): 5-19, 1992.

28. Ting, K. and Long, Y.: "Performance Quality and Tolerance Sensitivity of Mechanisms." *Transactions of the ASME, Journal of Mechanical Design,* **118**: 144-150, 1996.

29. Waldron, K. and Kumar, V.: "Development of a Theory of Errors for Manipulators." *Proceedings of the Fifth World Congress on the Theory of Machines and Mechanisms* : 821-826, 1979.

30. Wu, C.: "A Kinematic CAD Tool for the Design and Control of a Robot Manipulator." *The International Journal of Robotics Research,* **3**(1): 58-67, 1984.

31. Vaichav, R. and Magrab, E.: "A General Procedure to Evaluate Robot Positioning Errors." *The International Journal of Robotics Research,* **6**(1): 59-74, 1987.

32. Veitchegger, W. and Wu, C.: "Robot Accuracy Analysis Based on Kinematics." *IEEE Journal of Robotics and Automation,* **RA-2**(3): 171-179, 1986.

33. Zhuang, H., Roth, Z. and Hamano, F.: "A Complete and Parametrically Continuous Kinematic Model for Robot Manipulators." *IEEE Transaction in Robotics and Automation,* **8**(4): 451-462, 1992.

34. Zhuang, H., Wang, K. and Roth, Z.: "Optimal Selection of Measurement Configurations for Robot Calibration Using Simulated Annealing." *Proceedings of the IEEE 1994 International Conference in Robotics and Automation* : 393-398, San Diego, CA, 1994.

35. Ziegert, J., Olson, D., Datseris, P.: "Description of Machine Tool Errors Using Screw Coordinates," *Transactions of the ASME, Journal of Mechanical Design,* **114**: 531-535, 1992.

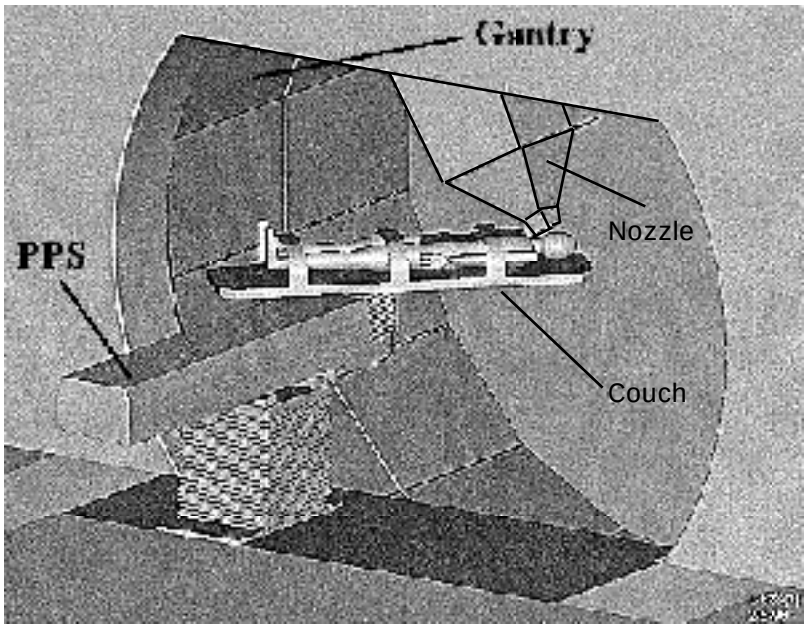

Figure 1: Schematic of the PPS, the Nozzle and the Gantry

Figure 1: Schematic of the PPS, the Nozzle and the Gantry

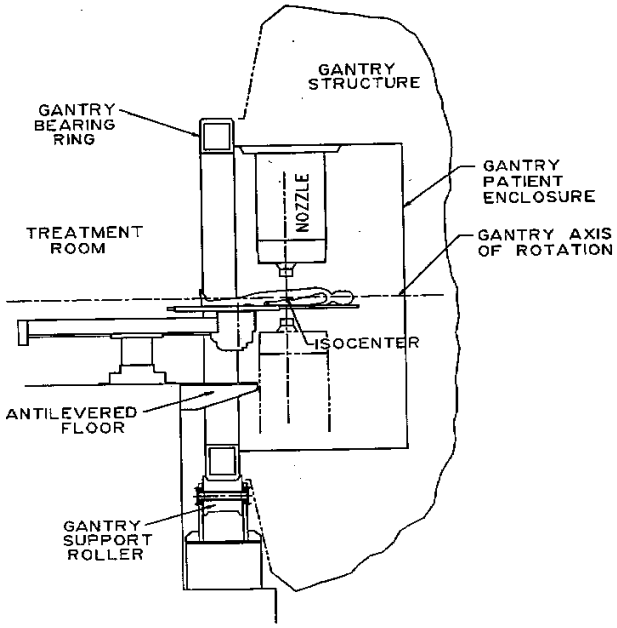

Figure 2: Side View of the Treatment Room [12, 13]

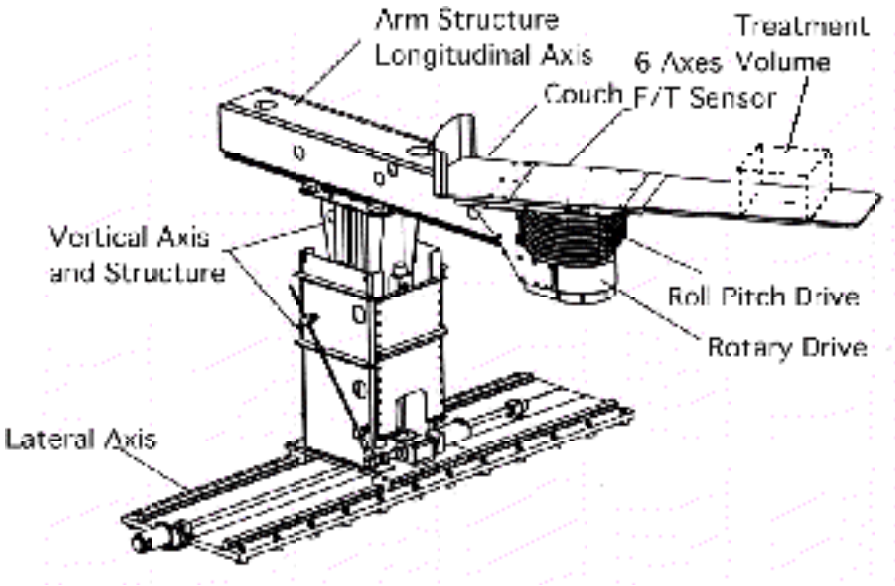

Figure 3: Close View of the Patient Positioning System [13]

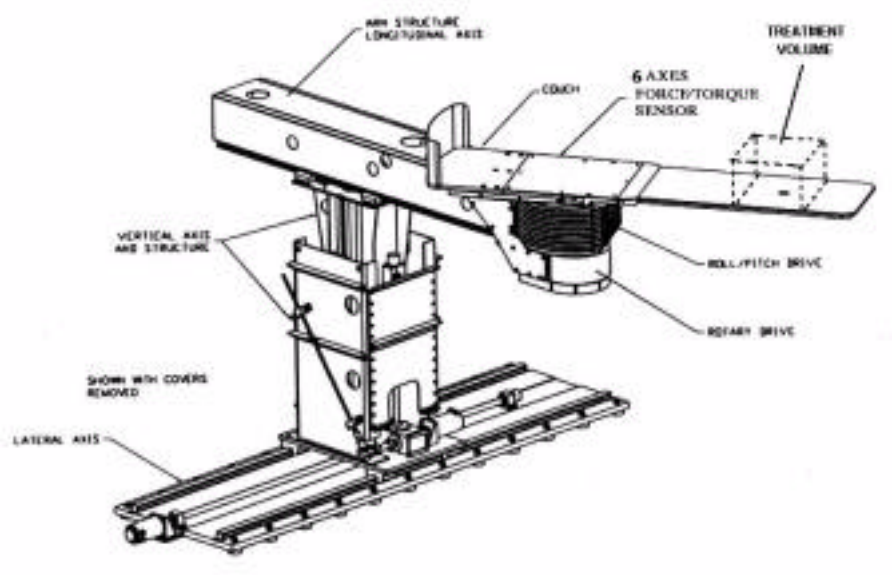

Figure 3: Close View of the Patient Positioning System [13]

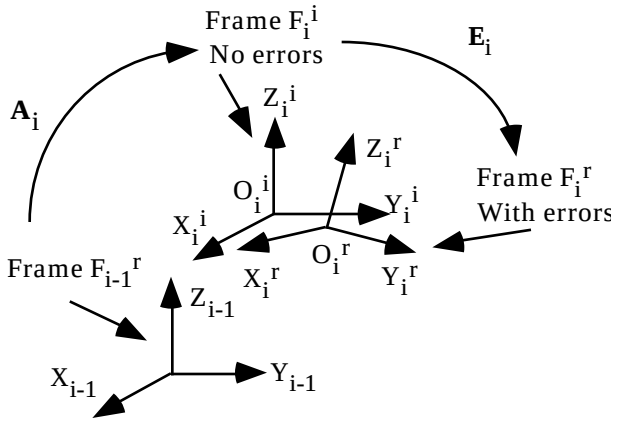

Figure 4: Frame Displacement Due to Errors

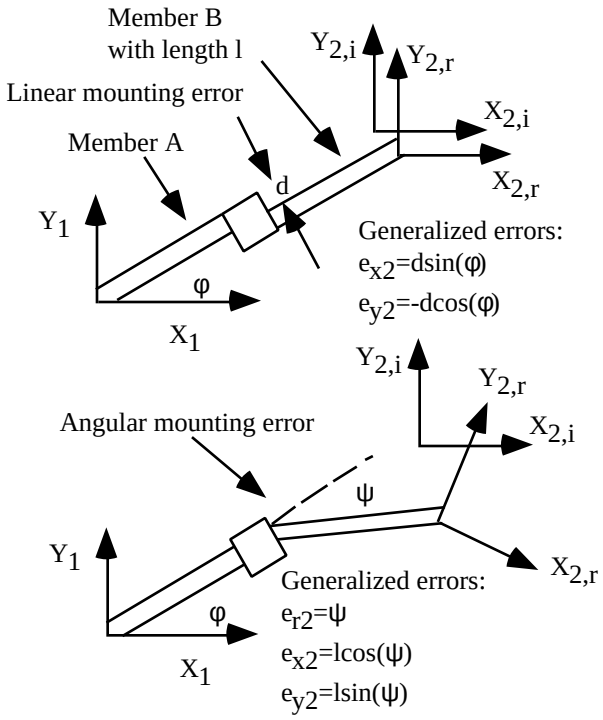

Figure 5: Generalized Error Calculation

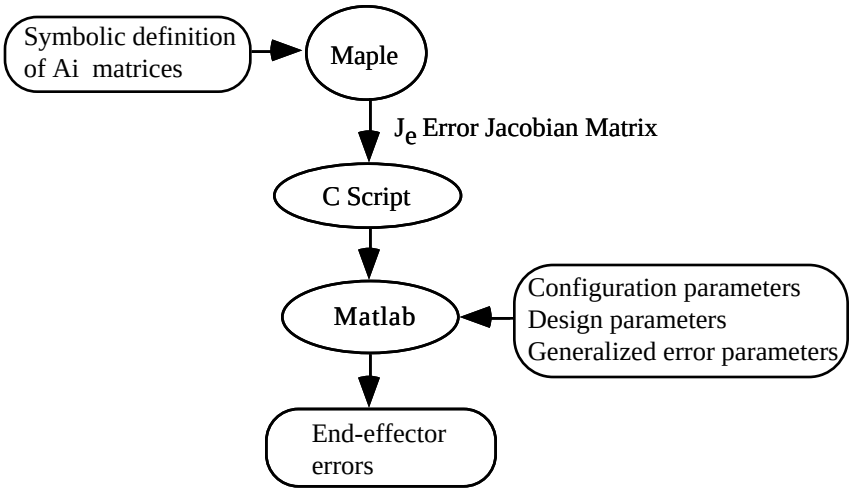

Figure 6: Error Analysis Program

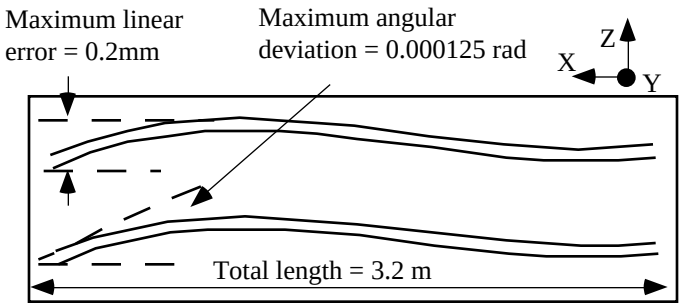

Figure 7: Base Rail Curvature Error of the PPS

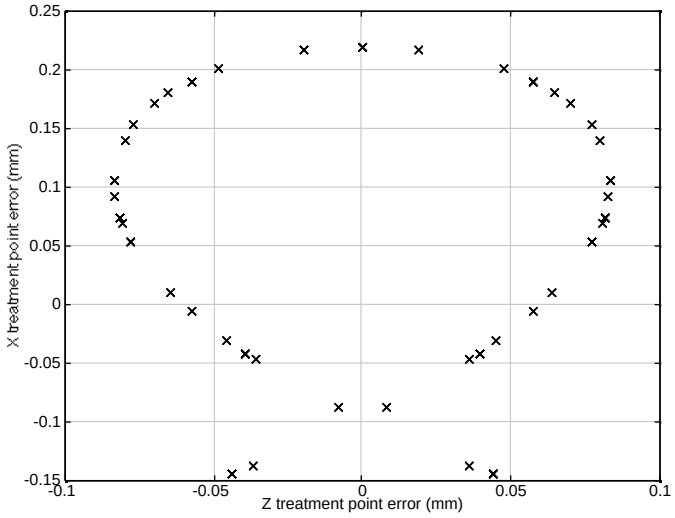

Figure 8: Effect of Base Rail Curvature

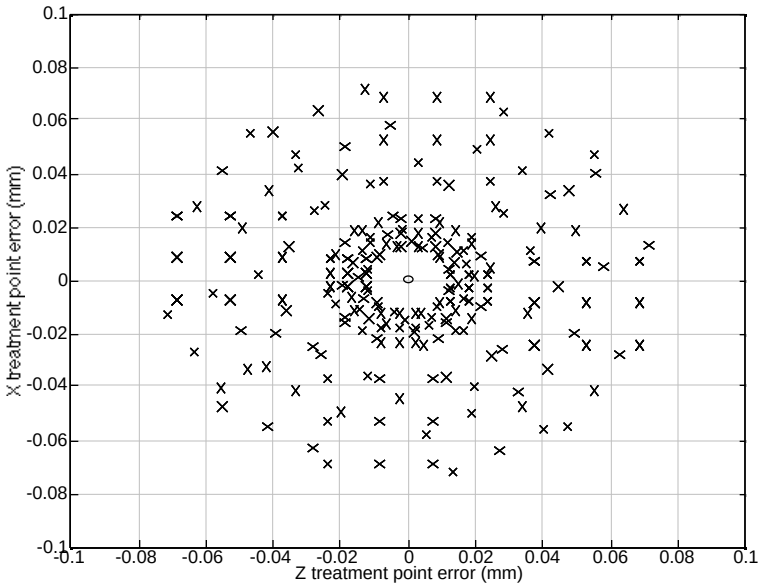

Figure 9: Effect of Encoder Measurement Error

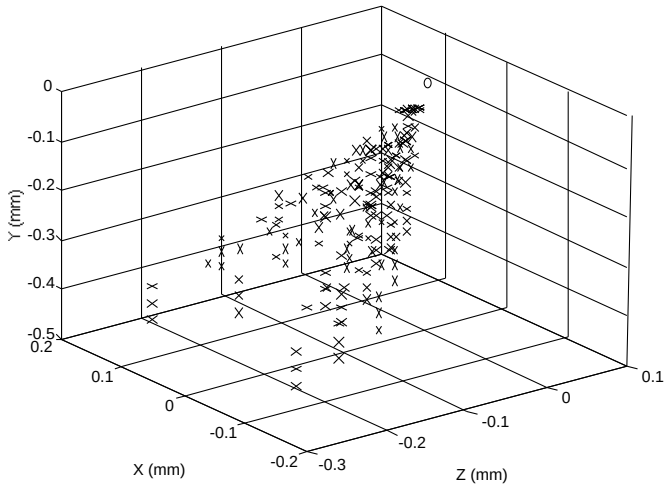

Figure 10: Effect of Deflections of the Arm

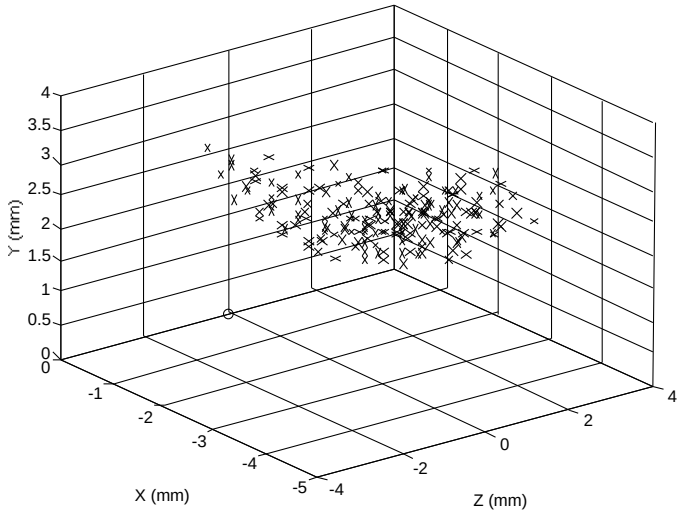

Figure 11: Sum of the Treatment Point Errors

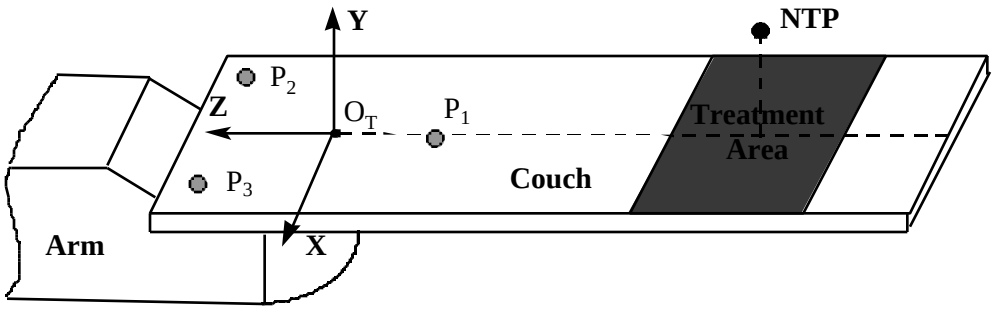

Figure 12: Close View of the Couch

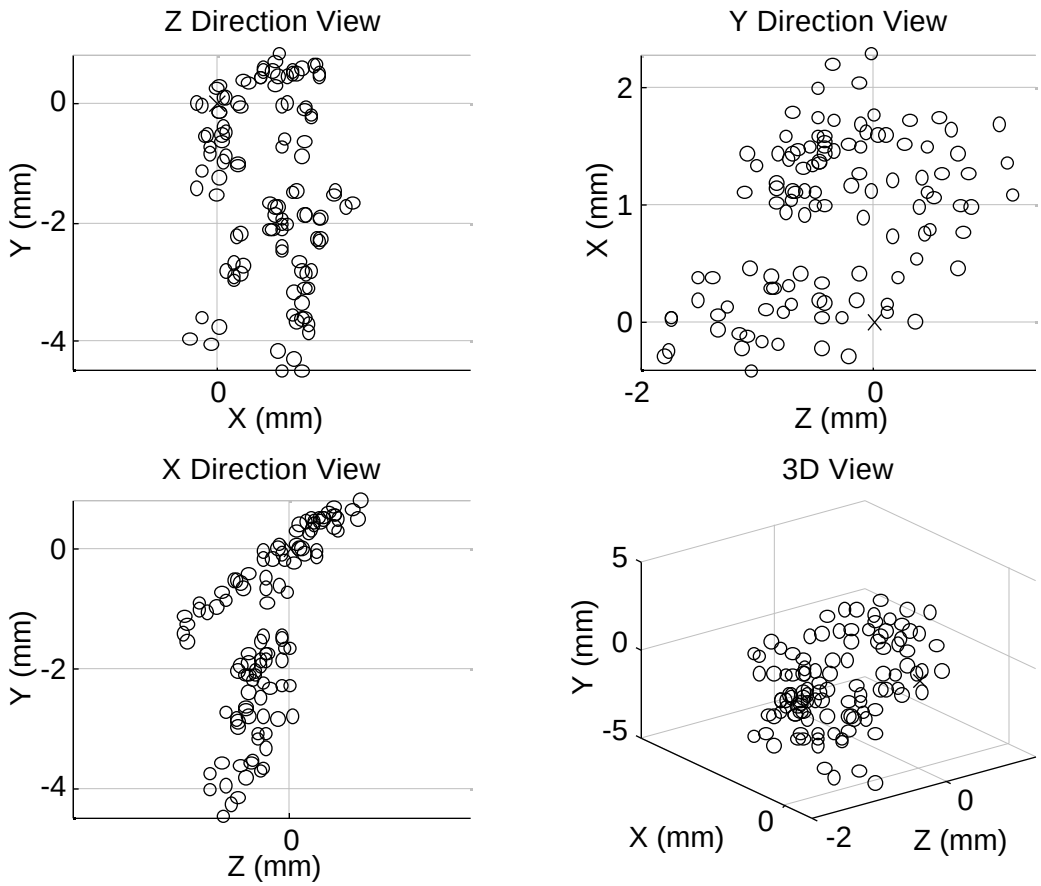

Figure 13: Accuracy of the PPS Based on Experimental Measurements

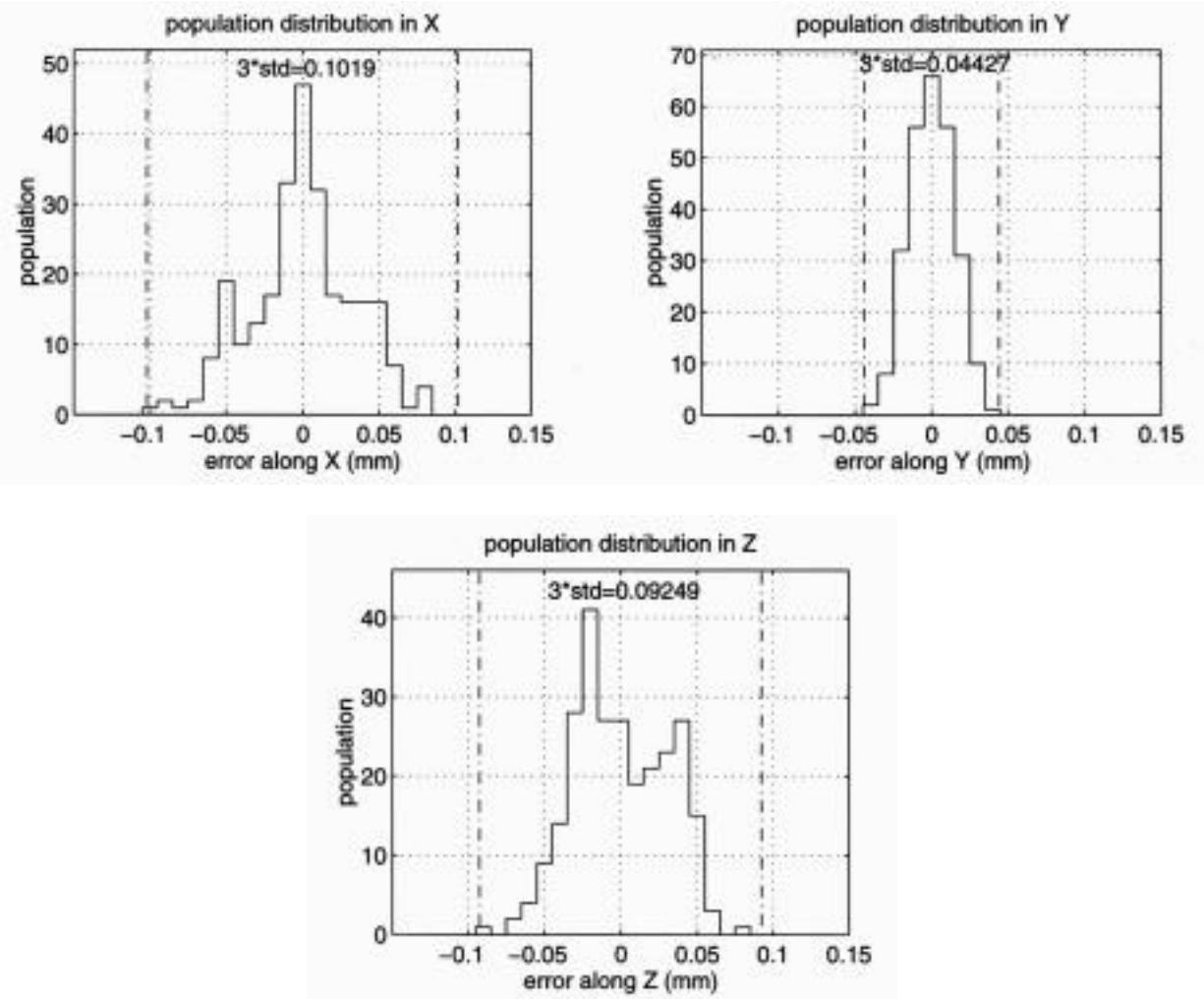

Figure 14: Repeatability Distribution Based on Experimental Measurements